# Title: Recombinant Spidroins Fully Replicate Primary Mechanical Properties of Natural Spider Silk

***Authors:*** *Christopher H. Bowen,[1 †], Bin Dai[1, †], Cameron Sargent[1], Wenqin Bai[1], Pranay Ladiwala[1], Huibao Feng[1], Wenwen Huang[3], David Kaplan[3], Jonathan Galazka[4], Fuzhong Zhang[1,2, *]*

**Affiliations:**

[1]Department of Energy, Environmental and Chemical Engineering,

[2] Institute of Materials Science & Engineering,

Washington University in St. Louis, Saint Louis, MO 63130, USA

[3] TBA

[4] Space Biosciences Division, Ames Research Center, National Aeronautics and Space Administration, Mountain View, CA 94035, USA

[†] These authors contributed equally.

[*]Correspondence to: fzhang@seas.wustl.edu

**Abstract:**

**Dragline spider silk is among the strongest and toughest bio-based materials, capable of outperforming most synthetic polymers and even some metal alloys.[1,2,3,4] These properties have gained spider silk a growing list of potential applications that, coupled with the impracticalities of spider farming, have driven a decades-long effort to produce recombinant spider silk proteins (spidroins) in engineered heterologous hosts.[2] However, these efforts have so far been unable to yield synthetic silk fibers with mechanical properties equivalent to natural spider silk, largely due to an inability to stably produce highly repetitive, high molecular weight (MW) spidroins in heterologous hosts.[1,5] Here we address these issues by combining synthetic biology techniques with split intein (SI)-mediated ligation for the bioproduction of spidroins with unprecedented MW (556 kDa), containing 192 repeat motifs of the *Nephila clavipes* MaSp1 dragline spidroin. Fibers spun from these synthetic spidroins display ultimate tensile strength (σ), modulus (E), extensibility (ε), and toughness ($U_T$) of 1.03 ± 0.11 GPa, 13.7 ± 3.0 GPa, 18 ± 6%, and 114 ± 51 MJ/m$^3$, respectively—equivalent to the performance of natural *N. clavipes* dragline silk.[6] This work demonstrates for the first time that microbially produced synthetic silk fibers can match the performance of natural silk fibers by all common metrics (σ, E, ε, $U_T$), providing a more dependable source of high-strength fibers to replace natural spider silks for mechanically demanding applications. Furthermore, our biosynthetic platform can be potentially expanded for the assembly and production of other protein-based materials with high MW and repetitive sequences that have so far been impossible to synthesize by genetic means alone.**

**Main Text:**

Dragline spidroins are typically very large (200-350 kDa), highly repetitive proteins, containing hundreds of tandem repeats of glycine and alanine-rich sequences.[1,7] As with most polymers, the size of these spidroins is expected to positively correlate with tensile strength due to an increased density of interchain interactions and entanglements and fewer chain-end defects.[8,5] Indeed, previous work has demonstrated a clear correlation between MW and strength for recombinant *N. clavipes* dragline fibers, with the largest spidroin (96-mer, 285 kDa) yielding the strongest recombinant fiber reported to date (~550 MPa).[5] However, despite the apparent need for even larger spidroins to yield natural strength fibers (1.1 GPa for *N. clavipes* dragline)[6], dragline spidroins larger than 285 kDa have yet to be produced in quantities sufficient for fiber testing due to major challenges in recombinant production of high MW spidroins (e.g. instability of long, highly repetitive DNA/mRNA sequences in heterologous hosts, translation inhibition by complex mRNA secondary structures, high demands for glycine and alanine tRNAs, overall metabolic burden).[5]

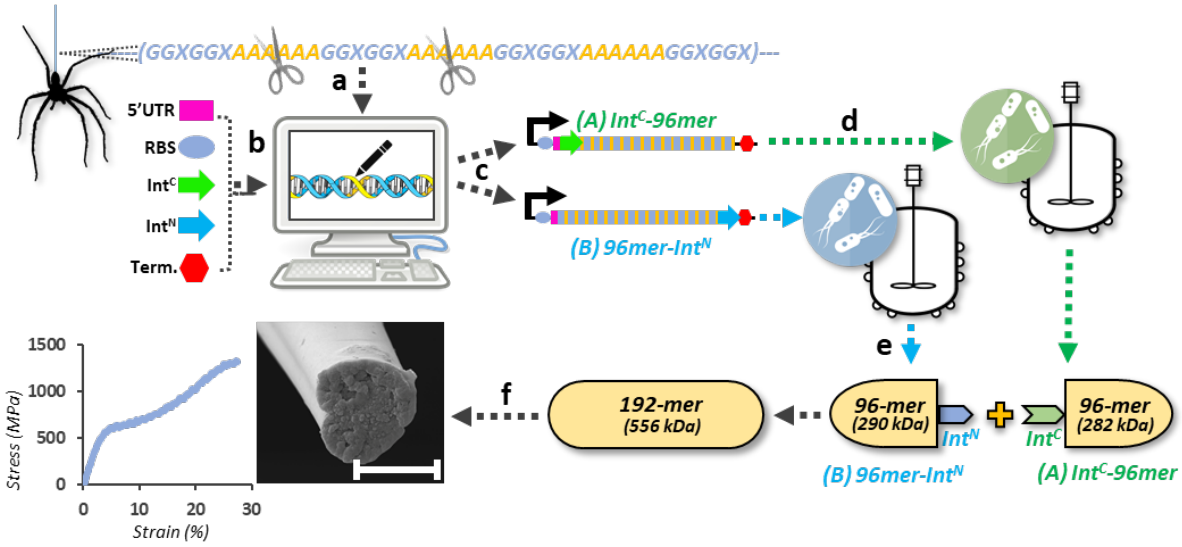


**Figure 1. Process schematic for split intein-mediated ligation of spider silk proteins with unprecedented molecular weight and mechanical properties. (a)** The highly repetitive core of natural *N. clavipes* dragline silk protein MaSp1 (shown as an idealized peptide sequence) is reduced to a single repeat unit (1-mer). **(b)** The 1-mer DNA sequence is combined *in silico* with 5' UTR, RBS, and split intein (SI) sequences, which are then computationally optimized for microbial production. **(c)** The optimized DNA sequences are assembled through our standardized SI-Brick system to yield complementary $Int^C$- or $Int^N$-flanked 96-mer constructs which are **(d)** transformed to *E. coli* for bioproduction. **(e)** Cell cultures are mixed and lysed to initiate SI-mediated covalent ligation of 96-mer spidroins to yield a 192-mer, 556 kDa product. **(f)** Ligated product is purified and spun into fibers for mechanical testing. Scale bar indicates 5 µm.

To confront these challenges, we envisioned using split intein (SI)-mediated reactions to post-translationally ligate the largest spidroins that can be stably expressed in engineered *Escherichia coli* (i.e. 96-mer, Fig. 1). SIs are peptide auto processing domains that, when fused

to separately expressed proteins, catalyze spontaneous splicing reactions, covalently linking their fusion partners via a peptide bond and leaving only a few residues (6 amino acids in this case) at the ligation site.[9] In this context, these residues are unlikely to affect the properties of the much larger ligated spidroins (6720 amino acids). Given the tendency of large silk sequences to form inclusion bodies in microbial hosts, we employed a recently engineered SI pair (Cfa) that retains catalytic activity in the presence of 8 M urea, a denaturant often used to extract and solubilize spidroins from heterologous hosts.[10] Thus, ligating an N-intein fused 96-mer ($^{N}96$) with a C-intein fused 96-mer ($96^{C}$) spidroin would yield a 556 kDa, 192-mer spidroin (Fig 1e).

To facilitate microbial production of highly repetitive, SI-fused material proteins, we developed a standardized DNA assembly strategy, termed SI-Bricks (Supplementary Note 1 and Figure 1). The SI-Bricks strategy allows for rapid genetic swapping of the core components of the devised SI-mediated ligation system (e.g. N-inteins, material proteins, C-inteins, and fusion domains/purification tags) in addition to common standardized biological parts (e.g. promoters, ribosomal binding sites, replication origins, and selection markers), all through simple restriction enzyme digestion/ligations. With SI-Bricks, starting from a single codon-optimized repeat unit (1-mer) of the *N. clavipes* dragline spidroin MaSp1, we assembled 64-mer and 96-mer spidroin DNA sequences by iterative end-to-end restriction digestion/ligation. The spidroin sequences were then genetically combined with codon-optimized SI DNA sequences and expression parts (Supplementary Figure 2). The resulting SI-fused spidroins ($^{N}64$, $64^{C}$, $^{N}96$, and $96^{C}$) were individually expressed in an *E. coli* host with $^{glycyl}$tRNA levels engineered to meet the demands of the most frequently used glycine codons in the spidroin sequences (Methods). Following our optimized fermentation conditions (Methods), typical titer of the SI-fused spidroins was nearly 2

g/L from glucose minimal medium with tryptone supplementation after four hours of production (Supplementary Figure 3).

Spidroin inter- and intramolecular interactions are highly sensitive to salt and pH, even in the presence of 8 M urea, and we expected that unwanted spidroin interactions would lower SI ligation efficiency. Thus, to test optimum conditions for ligation of SI-fused spidroins, 8 M urea extracts of *E. coli* expressing $64^{N}$ or $^{C}64$ were mixed at several salt concentrations, temperatures, and pH values (Extended Data Figure 1). Under all tested conditions, SI-mediated spidroin ligation is both rapid and robust, with the highest ligation yields observed at 37 °C, 300 mM NaCl, pH 7. Thus, for all subsequent ligations, these conditions were maintained, giving ligation yields of 68% and 62% for 128-mer and 192-mer spidroin, respectively (Extended Figure Data Figure 2). Ligation products were separated from most cellular proteins by selective precipitation with ammonium sulfate and further separated from unreacted 64-mer or 96-mer by size exclusion chromatography (SEC) for a final product purity ≥90% (Supplementary Fig. 4). As a standard for mechanical properties, a 96-mer spidroin with no SIs was also expressed and purified following identical procedures. All purified proteins were lyophilized and dissolved in hexafluorisopropanol (HFIP) to yield 14% w/v spinning dopes which were wet-spun into solid fibers by extrusion into a 95% methanol bath followed by immediate post-spin drawing.

Mechanical testing of post-drawn fibers revealed significant, nearly two-fold increases in both tensile strength (from 525 ± 83 MPa to 1031 ± 111 MPa, $P < 0.0001$, n=14) and modulus (from 7.8 ± 1.3 GPa to 13.7 ± 3.0 GPa, $P < 0.0001$, n=14) between 96-mer and 192-mer fibers (Fig. 2a,b). Average toughness also increased slightly (25%), while average breaking strain decreased slightly (22%), though neither change is statistically significant due to large fiber to fiber variations (Fig. 2c, d). For both strength and modulus, 128-mer fibers showed performance

intermediate to 96- and 192-mer fibers. Together, these results strongly suggest that there remains a positive correlation between spidroin size and fiber strength and modulus up to a MW of at least 556 kDa. Most significantly, these results demonstrate that fibers spun from a microbially synthesized 192-mer *N. clavipes* dragline spidroin have mechanical properties equivalent to natural *N. clavipes* dragline silk (i.e., $\sigma = 993 \pm 140$ GPa, $E = 14.0 \pm 4.0$ GPa, $U_T = 111.2 \pm 30$ MJ/m$^3$, $\varepsilon = 16.3 \pm 3.8\%$, Extended Data Table 1).[6,11,12,13]

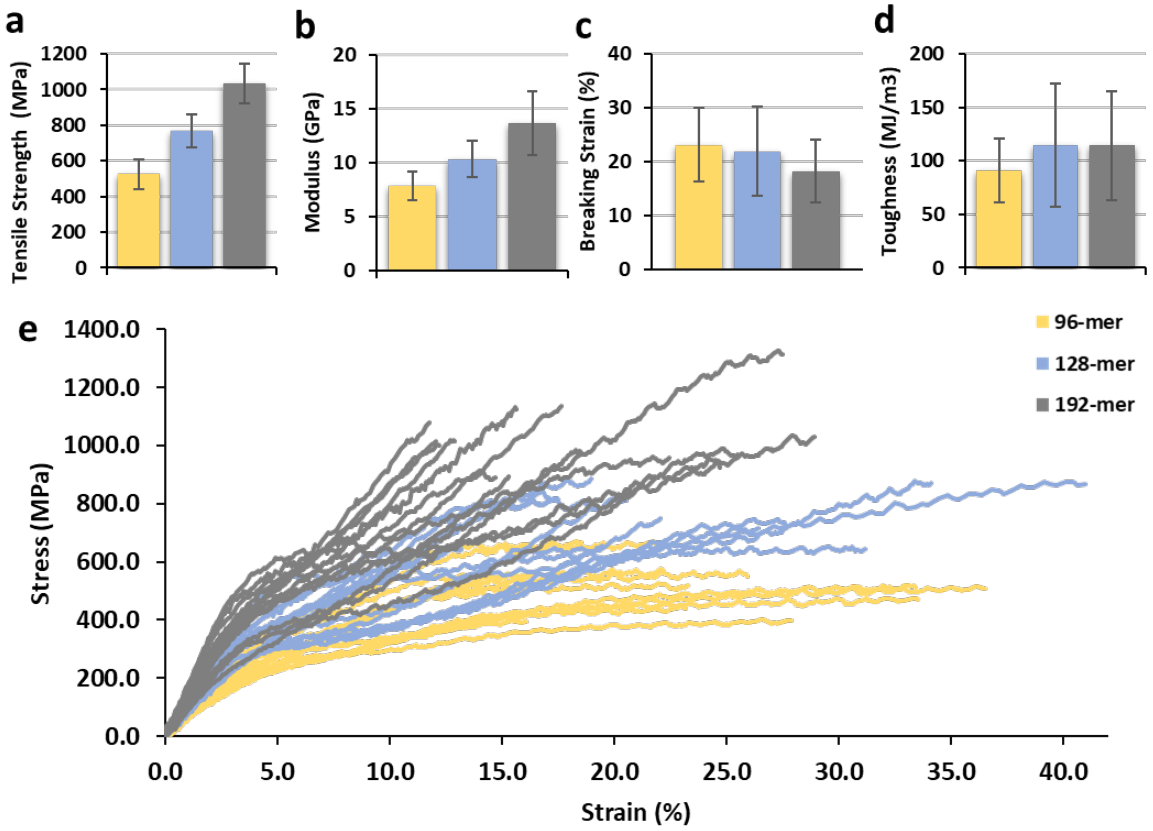


**Figure 2. Mechanical properties of synthetic silk fibers from high MW spidroins. (a)** Ultimate tensile strength, **(b)** elastic modulus, **(c)** breaking strain, and **(d)** toughness of 96-mer, 128-mer, and 192-mer fibers. All properties are calculated from stress-strain curves of 14 fibers for each MW. Error bars represent standard deviations, n = 14. **(d)** Compiled stress-strain curves for all fibers tested.

To gain insight into the origins of the exceptional strength and toughness of 192-mer fibers, we examined fiber physical characteristics at both micro and molecular scales. At the micro scale, light microscopy images confirmed that our fibers have consistent diameters along the fiber axes and that diameters do not vary significantly with MW ($P = 0.1389$, unpaired t test, Extended Data Table 1, Supplementary Fig. 5). Fiber diameters are also similar to those of natural dragline fibers, which have been reported to range from 1-8 μm (Supplementary Fig. 5).[12,11,14] Scanning electron microscopy (SEM) micrographs showed a distinct trend of decreasing surface roughness as well as fewer interior defects with increasing MW (Extended Fig. 3-5). To quantify this trend, fiber exterior and interior roughness were scored on a scale of 0-10, and mean roughness from six micrographs for each spidroin MW were calculated (Fig. 3b; Supplementary Table 7). By this metric, surface roughness decreased 74% and interior roughness decreased 39% between 96-mer and 192-mer fibers. Meanwhile, a trend of increased circularity with increasing MW is also apparent from the SEM micrographs, with 96-mer fibers exhibiting variations of a tri-lobed structure and 192-mer fibers exhibiting a mostly compact, nearly circular morphology. The average circularity values for 192- and 96-mer fibers were 0.89 (± 0.05) and 0.55 (± 0.14), with a perfect circle giving a value of 1 (see Methods for calculation) (Fig. 3b; Supplementary Table 7).

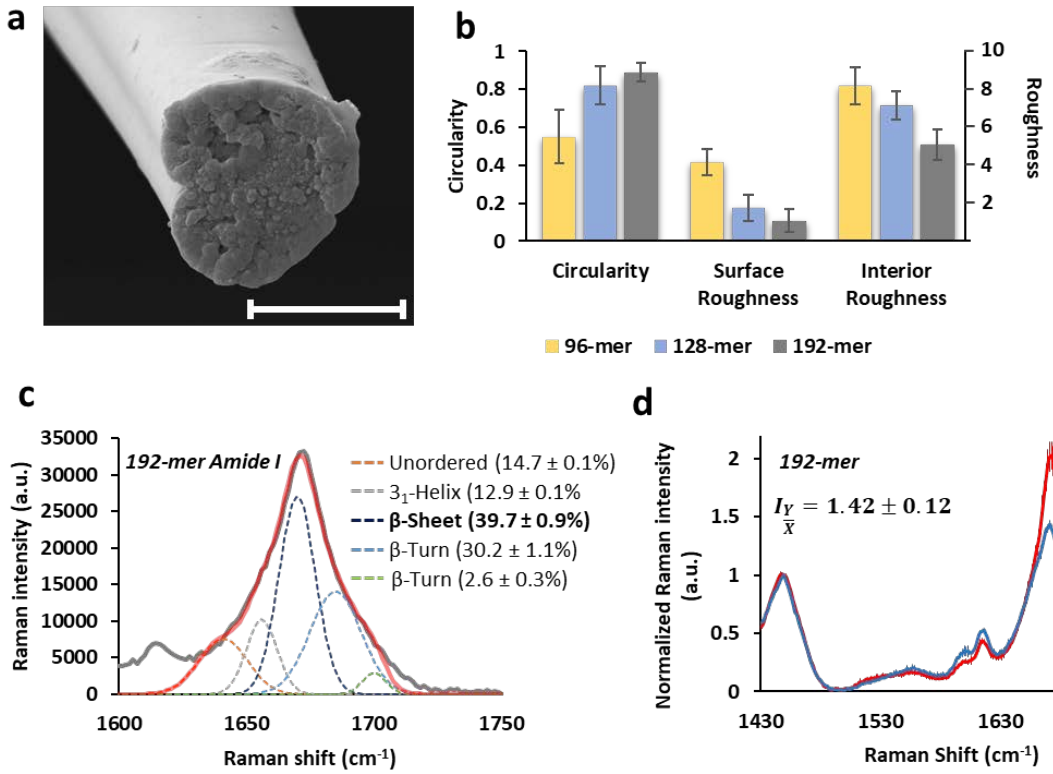


155

156 **Figure 3. Fiber characteristics at micro and molecular scales. (a)** Representative SEM
157 micrograph of a 192-mer fiber showing nearly circular cross-section, with smooth surface and
158 dense, relatively smooth interior morphology similar to natural dragline fibers. Scale bar is 5
159 µm. **(b)** Quantification of fiber circularity, surface roughness and interior roughness, showing
160 general trend of increasing circularity and decreasing roughness with increased fiber MW.
161 Measures are from micrographs presented in Extended Data Figure 3-5. **(c)** Representative
162 amide I band deconvolution and secondary structure quantification for 192-mer fibers showing
163 β-sheet content similar to natural dragline fibers. **(d)** Amide I Raman spectra for 192-mer fibers
164 oriented parallel (blue lines) or perpendicular (red lines) to the direction of laser polarization.
165 As expected for anisoptropic fibers with axial β-sheet crystal alignment, Amide I peak intensity

increases when fibers are oriented perpendicular to laser polarization (Supplementary Figure 6). Peak intensity ratio at 1670 $cm^{-1}$ ($I_{\frac{Y}{X}}$) is presented as an inset.

To further investigate fiber characteristics at the molecular scale, the 192-mer fibers were analyzed by polarized Raman microspectroscopy. Deconvolution of the amide I band (1630-1730 $cm^{-1}$) of Raman spectra confirm a high percentage (39.7 ± 0.9%) of β-sheet content in the 192-mer fibers (Fig. 3c), which agrees closely with β-sheet content (37 ± 3%) previously reported for natural *N. clavipes* dragline fibers as determined by both FTIR and polarized Raman.[15] Meanwhile, several studies have established that dragline fibers exhibit a high degree of chain alignment in the axial direction, with β-sheet crystals oriented parallel to the fiber axis—an important contributing factor to the exceptional tensile strength of dragline fibers.[16,17] Here, the β-sheet alignment along the fiber axis was measured by comparing the amide I β-sheet component (1670 $cm^{-1}$ peak intensities) between spectra acquired from fibers oriented both parallel (X-axis) and perpendicular (Y-axis) to the direction of laser polarization (Supplementary Fig. 6). The 192-mer fibers exhibited a peak intensity ratio ($I\frac{Y}{X}$) of 1.42 ± 0.12, which agrees closely to ratios previously reported for natural *N. clavipes* dragline fibers (1.59).[18] Overall, the β-sheet content and alignment observed here confirm that the synthetic 192-mer fibers are capable of recapitulating the structural characteristics of natural spider silk, which likely contributes to its observed mechanical performance.

Taken together, the synthetic silk fibers produced from our process not only display the key mechanical properties of natural silk but also characteristics including microscale morphology, β-sheet content, and axial alignment of β-sheet crystals. The observed relationship between spidroin MW and fiber strength suggest that spidroins larger than our 192-mer may

yield synthetic fibers even stronger than natural dragline silks. Additionally, integration of our biosynthetic process with recent advances in biomimetic spinning could further improve fiber performance and process simplification.

The fibers produced by this approach may accelerate the development of burgeoning markets that specifically demand high strength silk fibers, such as projectile protection in defense sectors, high strength lightweight cables and ropes in aerospace sectors, or high strength, monofilament, thin fibers ($\leq 10$ μm) for medical sutures. These applications are especially likely with further improvements in process yield. Moreover, the platform developed here can be easily expanded to other large and highly repetitive material proteins (e.g. collagens, elastins, sucker ring teeth proteins) for their microbial production from cheap and renewable feedstock.

**Full Methods** and any associated references are available in the online version of the paper at...

**Acknowledgements** We would like to thank Tavis Reed and Beryl Mpamo for their assistance with protein production; Srikanth Singamaneni, Sirimuvva Tadepalli, and Rohit Gupta for assistance with Raman microspectroscopy; and Xiaoxia Xia for suggestions on fiber spinning. We thank the Tianjin Institute of Industrial Biotechnology for providing the synthetic DNA sequence of *N. clavipes* MaSp1. This work was supported by a Young Investigator Program from AFOSR (FA95501510174 to FZ) and an Early Career Faculty grant from NASA's Space Technology Research Grants Program (NNX15AU45G to FZ).

**Author Contributions** F.Z. conceived the project. C.H.B. performed sequence/host optimizations, protein production, fiber spinning, and fiber characterizations. B.D. performed genetic assembly, protein production, and protein purification. C.S. performed SEM imaging. W.B. provided the original 1-mer sequence and production advice. P.L. and H.F. performed protein production. W.H. and D.K. provided training and advice in fiber spinning and characterization. J.G. provided advice and data analysis. C.B., C.S., and F.Z. prepared the manuscript.

**Author Information** The authors declare no competing financial interests. Correspondence and requests for materials should be addressed to F.Z. (fzhang@seas.wustl.edu).

## METHODS

**Strains and growth conditions.** *E. coli* NEB 10-beta (NEB10β) was used for all plasmid cloning and protein production. For all cloning, *E. coli* strains were cultured in Terrific Broth (TB) containing 24 g/L yeast extract, 20 g/L tryptone, 0.4% glycerol, 17 mM $KH_2PO_4$, and 72 mM $K_2HPO_4$ at 37°C with appropriate antibiotics (50 µg/mL kanamycin and 30 µg/mL chloramphenicol). M9 glucose medium with tryptone supplement (2% Glucose, 1x M9 Salts, 75 mM MOPS pH 7.4, 12 g/L tryptone, 5 mM Citrate, 2 mM $MgSO_4 \cdot 7H_2O$, 100 µM $FeSO_4 \cdot 7H_2O$, 100 µM $CaCl_2 \cdot 2H_2O$, 3 µM thiamine, 1x micronutrients [40 µM $ZnSO_4 \cdot 7H_2O$, 20 µM $CuSO_4 \cdot 5H_2O$, 10 µM $MnCl_2 \cdot 4H_2O$, 4 µM $H_3BO_3$, 0.4 µM $(NH_4)_6Mo_7O_{24} \cdot 4H_2O$, and 0.3 µM $CoCl_2 \cdot 6H_2O$]) was used for protein production in bioreactors.

**Chemicals and reagents.** Unless otherwise noted, all chemicals and reagents were obtained from Sigma-Aldrich (St. Louis, MO, USA). Plasmid purification and gel extraction kits

were purchased from iNtRON Biotechnology (Lynnwood, WA, USA). FastDigest restriction enzymes and T4 DNA ligase were purchased from ThermoFisher Scientific (Waltham, MA, USA) and used for all digestions and ligations following the manufacturer's suggested protocols.

**Genetic assembly of 64- and 96-mer spidroins.** The repeated spidroin DNA sequences were constructed using a method modified from previous work (Supplementary Figure 2). The coding sequence of 1-mer *N. clavipes* MaSp1 was obtained from Tianjin Institute of Industrial Biotechnology (Supplementary Table 1) and chemically synthesized by Integrated DNA Technologies (San Jose, CA, USA). This DNA sequence was flanked on the 5' end by restriction sites 5'-KpnI/NheI-3' and on the 3' end by restriction sites 5'-SpeI/Kpn2I-3'. The sequence was inserted between restriction site KpnI/Kpn2I of a medium copy (pBBR1 replication origin) chloramphenicol resistance (CmR) expression vector, resulting in plasmid p1. To begin the iterative DNA assembly, plasmid p1 was linearized by digestion with NheI and ligated with a second 1-mer sequence digested by NheI/SpeI. The ligation was transformed to NEB10β for amplification, yielding plasmid p2 containing 2-mer spidroin. The same procedure was repeated for p2, with insertion of a linearized 2-mer sequence, to yield plasmid p4. The process was repeated until p64 (32-mer + 32-mer) and p96 (64-mer + 32-mer) were obtained. Because the annealing of the NheI and SpeI complementary overhangs from joining fragments does not produce a new restriction site, digestion with NheI was used to confirm the proper orientation of the insert at each step based on fragment sizes.

**Construction and sequence optimization of silk-SI-fusion proteins.** N- and C-terminal SI amino acid sequences ($Cfa^N$ and $Cfa^C$, respectively) were obtained from a recent publication. SI coding sequences were optimized for *E. coli* expression along with 5'UTR and RBS sequences using a combination of computational approaches. Specifically, using the Gene Designer 2.0

(ATUM) software, a variable $Cfa^C$ coding sequence was flanked on the 3' end by invariable 5'-KpnI/NheI-3' restrictions sites and repetitive silk sequences, and on the 5' end by an invariable RBS/5'-UTR (5'-ATCAGCAGGACGCACTGACCGAATTCAAAAGATCTTTTAAGAAGGA GATATACAT-3'), including the 5'-EcoRI/BglII-3' restriction sites, and short peptide coding sequence 5'-ATGGCTAAGACTAAA-3' (for increased translation initiation rate, as described previously; Supplementary Table 1). Considering these flanking invariable sequences, the variable $Cfa^C$ sequence was optimized using a modified *E. coli* codon usage table and giving extra weight to 5' mRNA structure minimization during sequence optimization. The resulting sequence (Supplementary Table 1) containing the 5'UTR and $Cfa^C$ was synthesized as a gblock fragment by Integrated DNA Technologies and was inserted 5' of the 64-mer or 96-mer sequences by digestion/ligation with BglII/KpnI to yield plasmids $p^C64x$ and $p^C96x$, which encode fusion proteins $^C64$ and $^C96$, respectively (Supplementary Table 2). Similarly, the variable $Cfa^N$ sequence was flanked on the 5' end by invariable 5'-SpeI/Kpn2I-3' restrictions sites and on the 3' end by an invariable 5'-BamHI/XhoI-3' site and subjected to the same optimization process as $Cfa^C$. The resulting $Cfa^N$ sequence was synthesized and inserted 3' of the 64-mer and 96-mer sequences by digestion/ligation with Kpn2I/BamHI to yield plasmids $p64^N$ and $p96^N$, which encode fusion proteins $64^N$ and $96^N$, respectively. The resulting constructs allow for easy swapping of any $Int^C$ of interest by digestion with BglII/KpnI and any $Int^N$ of interest by digestion with Kpn2I/BamHI, while the presence of NheI/SpeI sites allows for iterative genetic assembly of any large or other repetitive material proteins of interest (Supplementary Figure 1).

**Upregulation of GlyV tRNA production.** In addition to sequence optimizations, cellular $^{glycyl}$tRNA levels were also upregulated to meet the high demands on $^{glycyl}$tRNA posed by spidroin overexpression. The glyV tRNA coding sequence and its native promoter were PCR-

amplified from the NEB10β genomic DNA (Supplementary Table 1) and cloned between AatII/XhoI sites of a medium copy vector carrying p15A replication origin and Kanamycin resistance ($Kan^R$), yielding plasmid pGlyV (Supplementary Table 2). For all spidroin expression, pGlyV was co-transformed with the spidroin plasmid.

**Shake flask cultures.** For initial ligation tests as shown in Supplementary Figures 2 & 4, protein production was carried out in shake flasks. Transformants were cultured overnight in 50 mL TB medium at 37 °C on an orbital shaker. Overnight 50 mL cultures were then inoculated into 500 mL fresh TB medium in Erlenmeyer flasks at an initial $OD_{600}$ = 0.08. Cultures were grown at 37°C with orbital shaking to $OD_{600}$ = 6, then induced by addition of 1 mM IPTG and cultured for an additional 6 hours at 30°C with orbital shaking.

**Bioproduction in fed-batch bioreactors.** All spidroins were finally produced in 2 L fed-batch bioreactors (Bioflo120, Eppendorf). Transformants were cultured overnight in 50 mL TB medium at 37°C on an orbital shaker. The overnight cultures were then inoculated into 1 L glucose M9 medium with tryptone supplement with an initial $OD_{600}$ = 0.08. After overnight incubation at 37°C with orbital shaking, 1 L cultures were pelleted by centrifugation at 4500 x g for 10 min and resuspended in 300 mL sterile resuspension medium (250 mM MOPS pH 7.4, 2.5% glucose, 60 g/L tryptone, 25 mM citrate, 10 mM $MgSO_4$, 500 µM $FeSO_4 \cdot 7H_2O$, 15 µM thiamine, 5x micronutrients). The resuspended cultures were then added to an autoclaved 2 L Bioflo120 heat-blanketed bioreactor containing 1.2 L water and 1.15x M9 salts. Sterile $CaCl_2 \cdot 2H_2O$ was added to a final concertation of 100 µM. Antifoam 204 was added as needed to minimize foaming (approximately 0.01%). Agitation and air flow was regulated to maintain approximately 70% dissolved oxygen (DO). After consumption of the initial 0.5% glucose (as judged by ΔDO), a sterile substrate feed (20% glucose, 48 g/L tryptone, and 10 g/L

303 $MgSO_4 \cdot 7H_2O$) was initiated to maintain a linear growth rate. Reactors were induced at $OD_{600}$ =
304 80 by addition of 1 mM IPTG and culture temperature was reduced to 30°C. Cultures were
305 collected four hours after induction. Titers were estimated from densitometric analysis of
306 Coomassie Blue-stained SDS-PAGE gels (Supplementary Figure 3).

307 **Protein ligation.** Cell cultures were pelleted by centrifugation at 4500 x g for 30 min.
308 Pellets from complimentary SI-fused spidroins (e.g. $96^N$ and $^C96$ or $64^N$ and $^C64$) were combined
309 at a 1:1 reactant ratio based on densitometric analysis of Coomassie Blue-stained SDS-PAGE
310 gels. Mixed pellets were resuspended in sonication buffer (300 mM NaCl, 20 mM MOPS pH
311 7.4, 2 mM TCEP, 1 mM PMSF) and sonicated using a QSonica Q700 sonicator (Qsonica,
312 Newton, CT, USA) for 10 min. Sonicated resuspensions were pelleted by centrifugation at
313 25,000 x g for 30 min to remove supernatants. Pellets were resuspended in ligation buffer (8 M
314 urea, 20 mM MOPS pH 7.4, 300 mM NaCl, and 2 mM TCEP) and stirred at 37°C for 24 h to
315 dissolve SI-fused spidroins and allow maximal ligation yield. The mixtures were then
316 centrifuged at 25,000 x g for 1 h to remove cell debris and undissolved proteins.

317 **Protein purification.** The purification protocol was modified from previous methods.
318 Specifically, ligated spidroins in ligation buffer were acidified with acetic acid to pH 4.0.
319 Ammonium sulfate was then added to a final concentration of 1.2 M. The mixture was then
320 centrifuged at 40,000 x g for 30 min. The pellet was discarded, and additional ammonia sulfate
321 was added to the supernatant to a final concentration of 2.3 M. After stirring for 1 h, the mixture
322 was centrifuged again at 40,000 x g for 15 min. The supernatant was discarded, and the pellet
323 was resuspended in SEC buffer (8 M urea, 10 mM ammonium bicarbonate pH 10) for further
324 purification by size-exclusion chromatography. SEC purifications were performed on an AKTA
325 Pure Chromatography System (GE Healthcare Life Sciences) using a HiPrep 16/60 Sephacryl S-

500 HR column (for 128-mer and 192-mer) or a HiPrep 16/60 Sephacryl S-400 HR column (for 96-mer). Proteins were separated using an isocratic elution with SEC buffer at a flow rate of 0.5 mL/min. Fractions containing greater than 90% ligation product, as determined by SDS-PAGE gel densitometry, were collected. SEC-purified fractions were combined and dialyzed in 10K MWCO SnakeSkin dialysis tubing (ThermoFisher Scientific) against 10 mM acetic acid aqueous solution. The dialyzed samples were then lyophilized.

**Ligation kinetics analysis.** For kinetics analysis, 64-mer protein concentrations in crude lysates were estimated by densitometric analysis of Coomassie Blue-stained SDS-PAGE gels. Based on estimated concentrations, fully sonicated resuspensions of $64^{C}$ and $^{N}64$ in ligation buffer were combined to give final concentrations of 100 µM for both $64^{C}$ and $^{N}64$ in a final volume of 500 µL. Combined resuspensions were pelleted by centrifugation, and pellets were resuspended in 500 µL of desired test buffer pre-incubated at the desired test temperature. Reactions were quenched by transferring 5 µL of reaction to 95 µL of Laemmli sample buffer preheated to 100°C and continuing boiling for 10 min.

**SDS-PAGE and densitometric analysis.** All SDS-PAGE gels were 1 mm thick, discontinuous with 3% stacking gel, and hand cast at the indicated percentages. Samples were prepared at 1 mg/mL or 5 µM total protein in Laemmli sample buffer (2% SDS, 10% glycerol, 60 mM Tris pH 6.8, 0.01% bromophenol blue, 100 µM DTT). Gels were run on Mini-PROTEAN Tetra Cells (Bio-Rad) in 1x Tris-glycine SDS buffer (25 mM Tris base, 250 mM glycine, 0.1% SDS), until just before the dye front exited the gel. Gels were stained in Coomassie Blue solution (50% methanol, 10% acetic acid, 1 g/L Coomassie Brilliant Blue) for a minimum of one hour at room temperature with gentle agitation and destained in Coomassie Blue destain buffer (40% methanol, 10% acetic acid) for a minimum of 1 hour. Gels were

imaged on an Azure c600 Imager (Azure Biosystems). All densitometry analysis was performed with the AzureSpot Analysis Software (Azure Biosystems). Images were background subtracted with an automatic valley-to-valley baseline detection. Protein band intensities were integrated by the software. Ligation yield was calculated as the intensity of the product band over the sum of both reactant and product band intensities. Spidroin titer was calculated as the intensity of the spidroin band over the sum of all band intensities multiplied by 150 mg/L/$OD_{600}$ and cell density at $OD_{600}$. (150 mg/L/$OD_{600}$ is the typical total protein titer in DH10β *E. coli* cells).

**Fiber spinning and mechanical testing.** Fiber spinning and mechanical testing were performed following a protocol modified from previous methods. Lyophilized spidroin powders were dissolved in hexafluorisopropanol (HFIP) to 14% w/v. This protein dope was loaded to a 100 µL Hamilton gastight syringe (Hamilton Robotics) fitted with a 23s gauge (116 µm inner diameter, 1.71 inch length) needle. The syringe was fitted to a Harvard Apparatus Pump 11 Elite syringe pump (Harvard Apparatus), and the dope was extruded into a 95% methanol bath at 5 µL/min (approximately 0.5 m fiber/min). Extruded fibers were then transferred to a 75% methanol bath and carefully extended at approximately 1 cm/s to the maximum draw ratio without fiber fracture (6x for 96-mer fibers, 9x for 128- and 192-mer fibers). Extended fibers were removed from the bath and held under tension until visibly dry. Segments of post-drawn fibers (20 mm) were carefully laid exactly vertical across a 5 mm square opening cut into a 20 mm square piece of cardstock and fixed with adhesive tape at both ends of the opening. Diameters of mounted fibers were then measured by light microscopy, averaging measurements at three points along the fiber axis. Mechanical properties were measured by axial pull tests on an MTS Criterion Model 41 universal test frame fitted with a 1N load cell (MTS Systems Corporation). Cardstock holders were mounted between two opposing spring-loaded grips, and

the supporting edges were carefully cut. Pull tests were conducted with a constant crosshead speed of 10 mm/min. Stress-strain curves were recorded by the MTS TW Elite test suite at a sampling rate of 50 Hz. Fiber breaks were recorded when a 90% drop from peak stress was detected. All mechanical properties were automatically calculated by the MTS TW Elite test suite. Ultimate tensile strength was calculated as the maximum measured load over the initial fiber cross-sectional area ($A = \pi r^2$), as determined from measured initial diameters. Modulus was calculated as the slope of a linear least squares fit to the stress/strain data of the initial elastic region. Toughness was calculated as the area under the total stress/strain curve divided by the initial fiber volume ($V = \pi r^2 h$) as calculated from measured initial fiber diameters and set initial gage length of 5 mm. For each protein, a total of 14 fibers were measured in this manner.

**Light microscopy.** Fiber diameters were measured using images acquired with a Zeiss Axio Observer ZI Inverted Microscope equipped with a 20x objective lens and the Axiovision LE software (Zeiss). For morphological analysis and further confirmation of fiber diameters, additional images were acquired with a Nikon Eclipse TiE Inverted Microscope equipped with a 60x objective and analyzed using the Nis-Elements software (Nikon).

**Scanning Electron Microscopy.** Following tensile tests, silk fibers were mounted onto a sample holder using conductive tape. The sample holder was sputter coated with a 10 nm gold layer using a Leica EM ACE600 high vacuum sputter coater (Leica Microsystems). Fibers were imaged using a Nova NanoSEM 230 Field Emission Scanning Electron Microscope (FEI) at an accelerating voltage of 7-10 kV. Fiber circularity was calculated from cross-sectional areas and perimeters as $4\pi(\frac{area}{perimeter^2})$, where a perfect circle gives a value of 1.

**Polarized Raman microspectroscopy.** Silk fibers were carefully fixed to glass microscope slides with microscale markings to ensure that spectra were acquired at the same

location before and after stage rotation. Raman spectra were acquired with a Renishaw RM1000 InVia Confocal Raman Spectrometer (Renishaw) coupled to a Leica DM LM microscope with rotating stage (Leica Microsystems). Silk fibers were initially oriented along the x-axis as depicted in Supplementary Figure 9. Fibers were irradiated at a fixed point with the 514 nm line of an argon laser with polarization fixed along the x-axis and focused through a 50x objective (NA = 0.75). Spectra were recorded from 1150-1750 $cm^{-1}$ with an 1800 lines/mm grating. For each acquisition, a total of 16 spectra were accumulated, each for 10 s. The stage was then rotated to orient fibers along the y-axis with the same laser polarization, and spectra were acquired a second time at the same fixed point. No signs of thermal degradation were apparent either visually or within recorded spectra. All recorded spectra were analyzed using the Fityk 0.9.8 software. Baselines were subtracted from all spectra using the built-in Fityk convex hull algorithm. For secondary structure determination, the amide I peak of y-axis oriented fibers was deconvolved into a set of five gaussian peaks centered at 1641, 1656, 1670, 1685, and 1700 $cm^{-1}$ for unordered, $3_1$-Helix, β-Sheet, β-Turn, and β-Turn components, respectively, as previously reported. Peak areas were integrated and percentages were calculated as the component peak area over the sum of all peak areas. Percentages were averaged from measurements of three fibers. For intensity ratio calculations, all spectra were normalized to the intensity of the 1450 $cm^{-1}$ peak, which arises from $CH_2$ bending and is insensitive to protein conformation. For each fiber, the normalized intensity at 1670 $cm^{-1}$ of the peak oriented along the Y-axis was divided by the normalized intensity of the peak oriented along the x-axis to give the intensity ratio ($I\frac{Y}{X}$). This procedure was performed on a total of three separate fibers and calculated intensity ratios were averaged. Spectra were also averaged and presented in Figure 3d with standard deviations for each point along the spectra.

**Extended Data Table 1. Averaged mechanical properties for fibers spun from synthetic spidroins compared to natural *N. clavipes* dragline fibers.**

| Spidroin | MW. (kDa) | Tensile Strength (MPa) [1] | Young's Modulus (GPa) [1] | Toughness ($MJ/m^3$) [1] | Breaking Strain (%)[1] | Diameter (μm) [1] | Source |
|---|---|---|---|---|---|---|---|
| Synthetic 96-mer | 277 | 525 ± 83 | 7.8 ± 1.3 | 91 ± 30 | 23 ± 7 | 6.3 ± 0.7 | Present study |
| Synthetic 128-mer | 373 | 767 ± 92 | 10.3 ± 1.7 | 115 ± 58 | 22 ± 8 | 6.6 ± 0.9 | Present study |
| Synthetic 192-mer | 556 | 1031 ± 111 | 13.7 ± 3.0 | 114 ± 51 | 18 ± 6 | 5.7 ± 1.3 | Present study |
| *Natural N. clavipes Dragline* | - | 950 ± 381 | 12 ± 5.2 | NA | 16.9 ± 5.2 | NA | Cunniff 1994 (Adapted from Zemlin, 1968) |
| *Natural N. clavipes Dragline* | - | 972 | 12.7 | NA | 18.1 | NA | Cunniff 1994 (Adapted from Zemlin, 1969) |
| *Natural N. clavipes Dragline* | - | 875 | 10.9 | NA | 16.7 | NA | Cunniff 1994 (Adapted from Zemlin, 1969) |
| *Natural N. clavipes Dragline* | - | 1100 | 22 | NA | 9 | 3.7 ± 0.8 | Cunniff, 1994 |
| *Natural N. clavipes Dragline* | - | 850 | 12.7 | NA | 20 | 4.2 | Ko, 2001 |
| *Natural N. clavipes Dragline* | - | 1215 ± 233* | 13.8 ± 3.6 | 111.2 ± 30 | 17.2 ± 3.5 | NA | Swanson, 2006 |
| *N. clavipes Dragline Average*** | | 993 ± 140 | 14.0 ± 4.0 | 111.2 ± 30 | 16.3 ± 3.8 | 3.7 ± 0.8 | Combined |

[1] For all mechanical measurements, n = 14.

* Swanson et al. reported "true" stress values rather than the more commonly reported "engineering stress" values. True stress calculates strength based on the final diameter of the fiber assuming constant volume deformation, thus true stress values are expected to be significantly higher than engineering stress values as calculated in the present study.

** Averaged from the six sources compiled in this table.

NA: values could not be found in the referenced study.

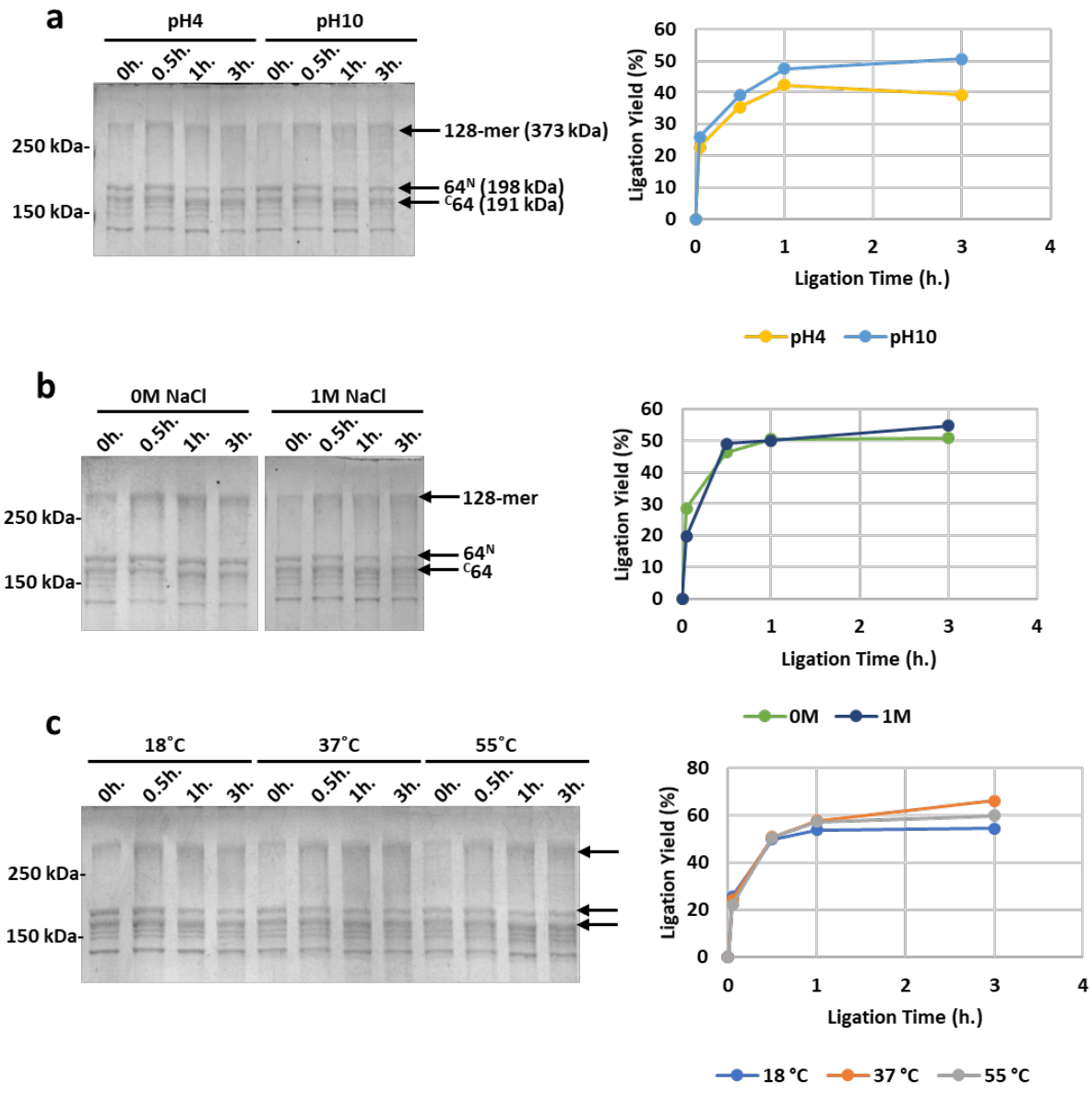


**Extended Data Figure 1. Kinetics of SI-catalyzed ligation of spidroins.** SDS-PAGE (left) of reaction mixtures containing 1:1 ratio of $64^{N}$ and $^{C}64$ in 8 M urea, 2mM TCEP at different pH **(a)** pH4 = (300 mM NaCl, 10 mM ammonium acetate pH 4); pH10 = (300 mM NaCl, 10 mM ammonium bicarbonate pH 10); different salt concentration **(b)** 0M = (0M NaCl, 10 mM MOPS pH 7.4); 1M = (1M NaCl, 10 mM MOPS pH 7.4); and different temperature **(c)** all buffers =

(300 mM NaCl, 10mM MOPS pH 7.4). Black arrows indicate the expected size of product and reactant bands. Ligation yields (right) were calculated as the area of the product band over the sum of both reactant and product bands. Note, spidroins used in this experiment were produced from shake flasks, which produce lower final titers than those from fed-batch bioreactors.

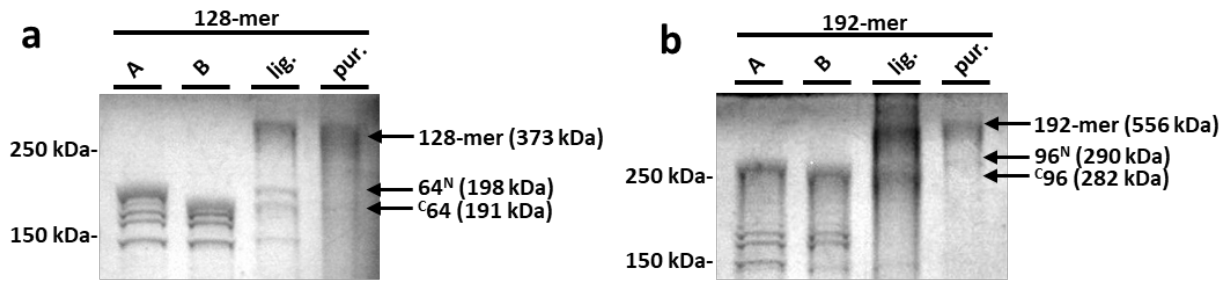


**Extended Data Figure 2. Ligation yields for 128-mer and 192-mer.** Coomassie Blue stained SDS-PAGE gels for **(a)** $64^{N}$ + $^{C}64$ ligation and **(b)** $96^{N}$ + $^{C}96$ ligation. Lane 1, whole cells expressing $Cfa^{N}$-fused spidroins ($64^{N}$ or $96^{N}$); lane 2, whole cells expressing $Cfa^{C}$-fused spidroins ($^{C}64$ or $^{C}96$); lane 3, ligation products after selective ammonium sulfate precipitation; lane 4, products after SEC purification.

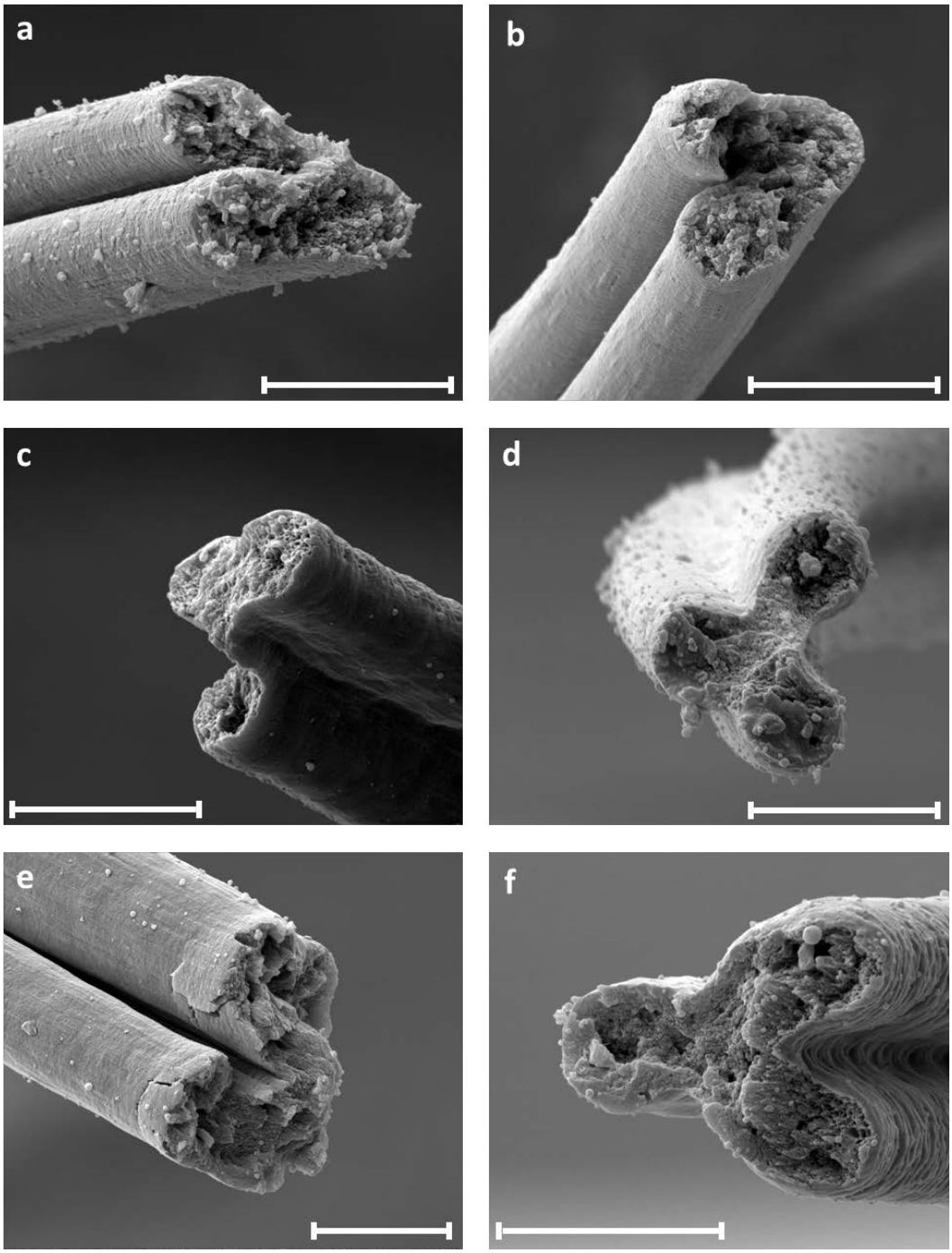


**Extended Data Figure 3. Representative SEM micrographs of 96-mer fibers.** All samples were taken after tensile tests. All scale bars are 5μm.

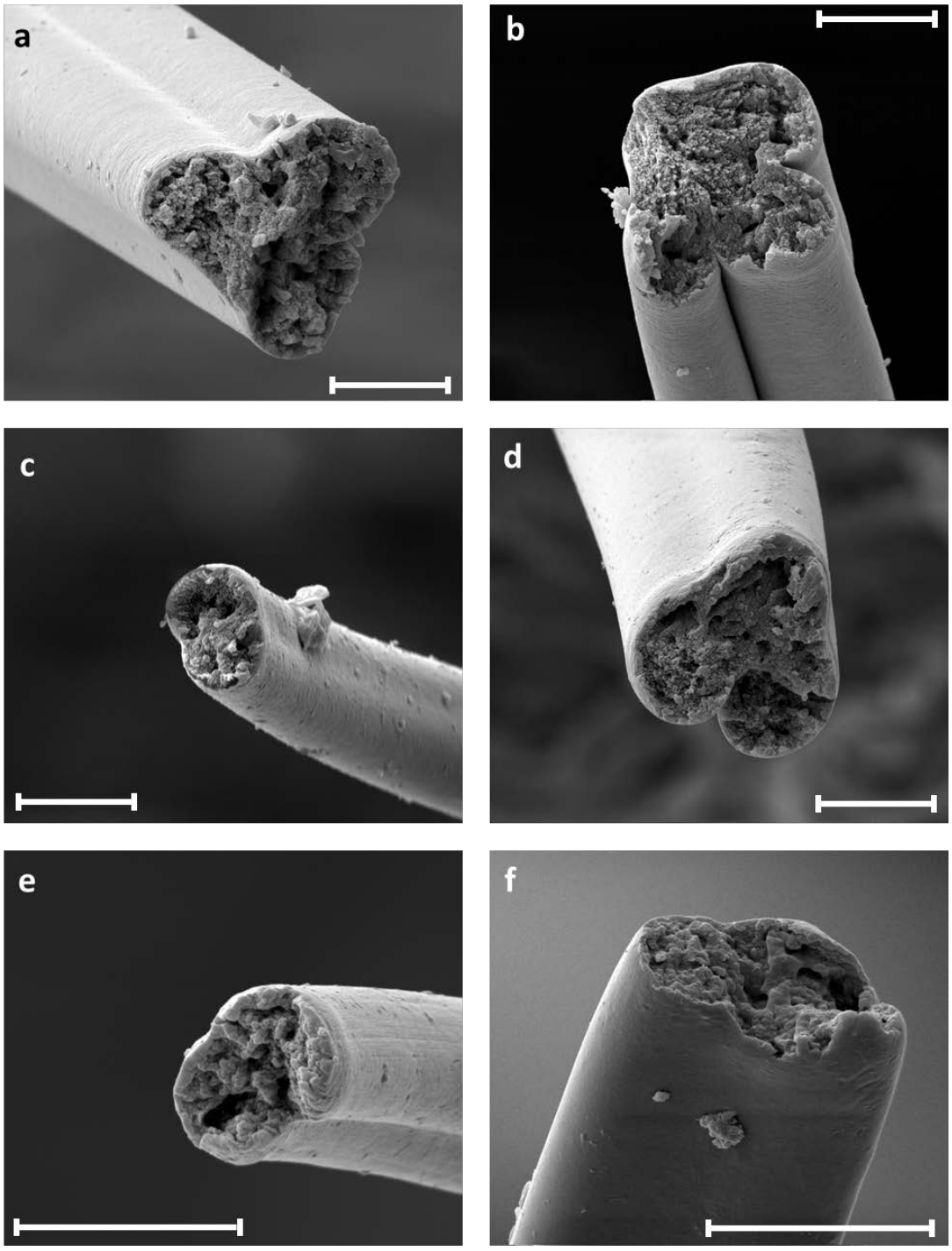


**Extended Data Figure 4. Representative SEM micrographs of 128-mer fibers.** All samples were taken after tensile tests. All scale bars are 5μm.

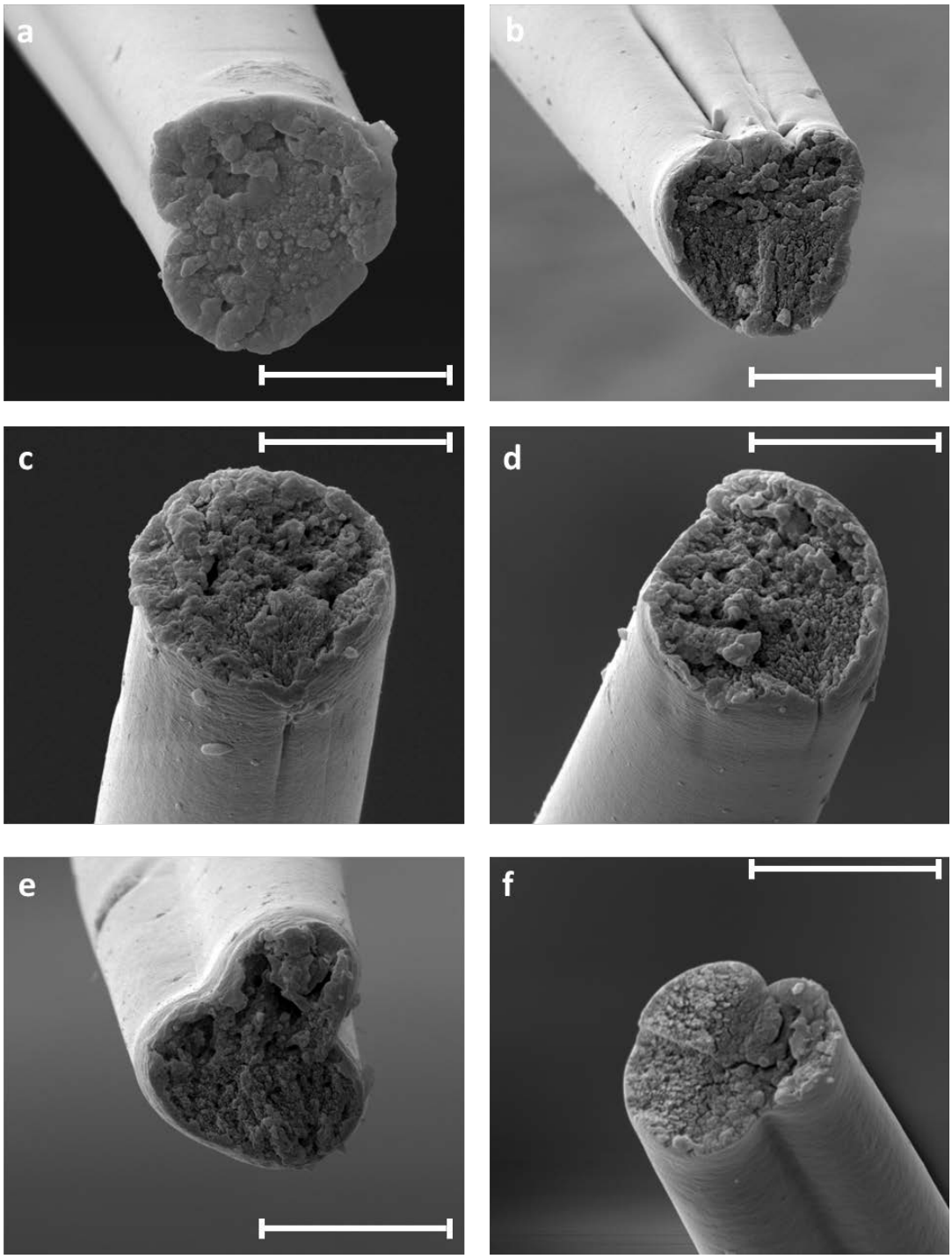


**Extended Data Figure 5. Representative SEM micrographs of 192-mer fibers.** All samples were taken after tensile tests. All scale bars are 5µm.

## REFERENCES


1. Omenetto, F. G. & Kaplan, D. L. New Opportunities for an Ancient Material. *Science.* **329,** 528–531 (2010).
2. Tokareva, O., Michalczechen-Lacerda, V. a., Rech, E. L. & Kaplan, D. L. Recombinant DNA production of spider silk proteins. *Microb. Biotechnol.* **6,** 651–663 (2013).
3. Heidebrecht, A. & Scheibel, T. *Recombinant Production of Spider Silk Proteins*. *Advances in Applied Microbiology* **82,** (Elsevier, 2013).
4. Teulé, F. *et al.* A protocol for the production of recombinant spider silk-like proteins for artificial fiber spinning. *Nat. Protoc.* **4,** 341–55 (2009).
5. Xia, X.-X. *et al.* Native-sized recombinant spider silk protein produced in metabolically engineered Escherichia coli results in a strong fiber. *Proc. Natl. Acad. Sci. U. S. A.* **107,** 14059–63 (2010).
6. Swanson, B. O., Blackledge, T. A., Summers, A. P. & Hayashi, C. Y. Spider Dragline Silk: Correlated and Mosaic Evolution in High-Performance Biological Materials. *Evolution (N. Y).* **60,** 2539 (2006).
7. Babb, P. L. *et al.* The Nephila clavipes genome highlights the diversity of spider silk genes and their complex expression. *Nat. Genet.* **49,** 895–903 (2017).
8. Nunes, Ronald; Martin, John; Johnson, J. Influence of Molecular Weight and Molecular Weight Distribution on Mechanical Properties of Polymers. *Polym. Eng. Sci.* **22,** 205–228 (1982).
9. Shah, N. H. & Muir, T. W. Inteins: Nature’s Gift to Protein Chemists. *Chem. Sci.* **5,** 446–461 (2014).
10. Stevens, A. J. *et al.* Design of a Split Intein with Exceptional Protein Splicing Activity. *J.*

*Am. Chem. Soc.* **138,** 2162–2165 (2016).

11. Zemlin, J. C. A study of the mechanical behavior of spider silks. *U.S. Army Natick Rep. AD-684 333* 1–68 (1968).

12. Cunniff, P. & Fossey, S. Mechanical and thermal properties of dragline silk from the spider Nephila clavipes. *Polym. …* **5,** 401–410 (1994).

13. Ko, F. K. *et al.* Engineering Properties of Spider Silk. *Mater. Res. Soc. Symp. Proc.* **702,** U1.4.1 (7 pages) (2001).

14. Prez-Rigueiro, J., Elices, M. & Llorca, C. V. Tensile properties of Argiope trifasciata drag line silk obtained from the spider's web. *J. Appl. Polym. Sci.* **82,** 2245–2251 (2001).

15. Lefèvre, T., Rousseau, M. E. & Pézolet, M. Protein secondary structure and orientation in silk as revealed by Raman spectromicroscopy. *Biophys. J.* **92,** 2885–2895 (2007).

16. Su, I. & Buehler, M. J. Nanomechanics of silk: the fundamentals of a strong, tough and versatile material. *Nanotechnology* **27,** 302001 (2016).

17. Prince, J. T., McGrath, K. P., DiGirolamo, C. M. & Kaplan, D. L. Construction, cloning, and expression of synthetic genes encoding spider dragline silk. *Biochemistry* **34,** 10879–10885 (1995).

18. Shao, Z., Vollrath, F., Sirichaisit, J. & Young, R. J. Analysis of spider silk in native and supercontracted states using Raman spectroscopy. *Polymer (Guildf).* **40,** 2493–2500 (1999).

**Supplementary Note 1. Design of SI-Brick DNA assembly system.** Our standardized SI-Brick DNA assembly system was developed based on five principle design considerations. (1) The system should allow for *in situ* iterative, back-to-back, genetic assembly of material protein repeat motifs up to the maximum genetically-permissible size. (2) The system should allow for selective swapping of the three standardized protein parts necessary for post-translational, SI-mediated ligation (i.e. RBS/$Int^N$, assembled material protein, and $Int^C$/stop codon). (3) No restriction sites within the coding sequence should introduce amino acids likely to be detrimental to SI ligation or protein material properties. (4) For maximum convenience, the platform should allow simultaneous "one-pot" assembly of all three protein parts. (5) The platform should also allow for selective swapping of the promoter, antibiotic marker, and replication origin.

We built our SI-Brick system (Supplementary Figure 1) based on existing BglBrick vectors which have been extensively used to construct multi-enzyme metabolic pathways for metabolic engineering.[1] The BglBrick vectors employ BglII and BamHI for digestion/ligation. However, the BglII and BamHI enzyme pair cannot be used to assemble material protein fragments because the resulting BglII site would introduce an arginine residue between SI and the material protein, proximal to the folded SI active site, which may negatively affect SI ligation, violating our design criterium (3). To solve this problem, we further incorporated an additional and orthogonal pair of restriction sites NheI and SpeI for iterative assembly of repetitive material protein sequences. NheI and SpeI code amino acids Alanine-Serine and Threonine-Serine, respectively, which should not affect SI ligation. During repetitive silk assembly, the scar sequence from NheI/SpeI ligation is ACTAGC, encoding a Threonine-Serine linker that is abundant in the native spidroin sequence and does not affect silk properties. Additionally, because existing BglBricks vectors already have SpeI for swapping of selection markers, flanking material proteins with NheI/SpeI alone would fail to meet criterium (2). Thus, we chose to flank material protein parts with an additional pair of restriction sites (KpnI and Kpn2I), allowing the repetitive proteins to be specifically swapped by enzyme pair KpnI and Kpn2I.

To use our SI-Brick DNA assembly system, repeat material protein motifs can be iteratively assembled through back-to-back digestion/ligation using NheI and SpeI (Supplementary Figure 2). The assembled material protein sequence can then be assembled with desired SI parts, promoters, vector backbones using corresponding restriction enzymes in one step (Supplementary Figure 2e). When needed, assembled repetitive proteins can be swapped with other material proteins with KpnI/Kpn2I digestion/ligation. Cfa $Int^C$ (including start codon and RBS) can be swapped with other $Int^C$ or N-terminal sequences with EcoRI/KpnI digestion/ligation. Cfa $Int^N$ can be swapped with other $Int^N$ with or without C-terminal purification tags using Kpn2I/BamHI digestion/ligation. Promoter parts can be swapped by AatII/EcoRI digestion/ligation, antibiotic markers together with replication origin can be swapped by AatII/XhoI. In addition, when needed, other proteins (e.g. a fluorescent reporter protein) can be cloned to the same operon with, but not genetically fused to, material proteins for tracking or regulation purposes using EcoRI/BglII or BamHI/XhoI digestion/ligation.

## Supplementary Table 1. Primers, UTRs, and coding sequences used in this study

| Primer/ UTR/ Coding Sequence | Name | Sequence | Purpose |
|---|---|---|---|
| 5'-UTR | NA | ATCAGCAGGACGCACTGACCGAATTCAAAAGATCTTTTAAGAAGGAGATATACAT | Previously optimized 5' UTR including strong RBS for high rate of translation inititiation |
| 3'-UTR | NA | GGATCCAAACTCGAGTAAGGATCTCCAGGCATCAAATAAAACGAAAGGCTCAGTCGAAAGACTGGGCCTTTCGTTTTATCTGTTGTTTGTCGGTGAACGCTCTCTACTAGAGTCACACTGGCTCACCTTCGGGTGGGCCTTTCTGCG | Previously optimized 3' UTR included two strong transcription terminators (rrnB T1 and T7Te) |
| CDS | MaSp1 1-mer | GGTACCGCTAGCGGTCGCGGTGGCCTGGGCGGTCAAGGTGCAGGTATGGCAGCAGCTGCAGCTATGGGTGGCGCTGGTCAAGGCGGTTATGGCGGTCTGGGTAGCCAAGGCACTAGTTCCGGA | Restriction site flanked 1-mer for assembly of 64-mer and 96-mer |
| CDS | $Cfa^N$ | TCCGGAGCAGAATATTGCCTGTCTTACGACACAGAGATTCTGACCGTTGAATATGGATTCCTTCCTATCGGTAAGATCGTGGAGGAACGGATTGAATGCACAGTCTATACGGTAGATAAAAATGGCTTTGTGTATACACAACCTATTGCTCAGTGGCATAACCGGGGAGAACAGGAAGTTTTCGAATACTGCTTAGAAGACGGTTCGATTATCCGTGCAACGAAAGATCACAAATTTATGACGACCGACGGTCAGATGTTACCGATTGATGAGATTTTCGAACGGGGGTTAGACCTGAAACAAGTTGATGGTTTGCCGTAAGGATCC | Final optimized C-terminal SI sequence for assembly with 64-mer or 96-mer silk sequences |
| CDS | $Cfa^C$ | AGATCTTTTAAGAAGGAGATATACATATGGCTAAGACTAAAGTCAAGATCATTAGTCGTAAGAGTCTGGGCACTCAAAACGTCTACGATATTGGAGTAGAAAAAGATCATAATTTTTTGCTGAAGAATGGGCTGGTGGCCTCTAACTGCTTCAACGGTACC | Final optimized N-terminal SI sequence for assembly with 64-mer or 96-mer silk sequences |
| Primer | GlyV-F | CGGAACGACGTCAATTTTTCCTGGTCACGTAAGCG | Amplification of GlyV from *E. coli* genome and cloning into pAk backbone |
| Primer | GlyV-R | GGCTACCTCGAGTTGGGTGGTCTGTGCTTTGCAG | Amplification of GlyV from *E. coli* genome and cloning into pAk backbone |

**Supplementary Table 2. Plasmids used in this study**

| Plasmid Name | ORI | Promoter | Resistance | Gene | Plasmid Source |
|---|---|---|---|---|---|
| pB6c | pBBR1 | $P_{LlacO1}$ | $Cm^R$ | - | Anderson et al. 2010[1] |
| p96 | pBBR1 | $P_{LlacO1}$ | $Cm^R$ | 96-mer | Present study |
| $p64^N$ | pBBR1 | pLlacO1 | $Cm^R$ | 64-mer + optimized 3' $Cfa^N$ | Present study |
| $p^C64$ | pBBR1 | pLlacO1 | $Cm^R$ | 64-mer + optimized 5' $Cfa^C$ | Present study |
| $p96^N$ | pBBR1 | pLlacO1 | $Cm^R$ | 96-mer + optimized 3' $Cfa^N$ | Present study |
| $p^C96$ | pBBR1 | pLlacO1 | $Cm^R$ | 96-mer + optimized 5' $Cfa^C$ | Present study |
| pA2k | p15A | $P_{Tet}$ | $Kan^R$ | - | JBE BioBrick paper |
| pGlyV | p15A | Native glyV,X,Y promoter | $Kan^R$ | Native *E. coli* glyV and promoter | Present study |

**Supplementary Table 3. Strains used in this study**

| Strain Name | Genotype | Strain Source |
|---|---|---|
| NEB10β | *F' proA+B+ lacIq Δ(lacZ)M15 zzf::Tn10 (TetR) Δ(ara-leu) 7697 araD139 fhuA ΔlacX74 galK16 galE15 e14- Φ80dlacZΔM15 recA1 relA1 endA1 nupG rpsL (StrR) rph spoT1 Δ(mrr-hsdRMS-mcrBC)* | NEB |
| s96 | NEB10β containing p96 + pGlyV | Present study |
| $s64^{N}$ | NEB10β containing $p64^{N}$ + pGlyV | Present study |
| $s^{C}64$ | NEB10β containing $p^{C}64$ + pGlyV | Present study |
| $s96^{N}$ | NEB10β containing $p96^{N}$ + pGlyV | Present study |
| $s^{C}96$ | NEB10β containing $p^{C}96$ + pGlyV | Present study |

**Supplementary Table 4. Diameter measurements and mechanical properties for 96-mer fibers**

| FIBER | Diam. A (μm) | Diam. B (μm) | Diam. C (μm) | Avg. Diameter (μm) | σ (MPa) | E (GPa) | ε (%) | $U_T$ (MJ/m³) |
|---|---|---|---|---|---|---|---|---|
| **1** | 6.53 | 6.22 | 5.57 | 6.11 | 566.7 | 7.4 | 25.4 | 110.0 |
| **2** | 5.89 | 6.22 | 5.58 | 5.90 | 526.6 | 7.6 | 21.8 | 90.0 |
| **3** | 7.80 | 7.33 | 7.48 | 7.54 | 401.3 | 5.6 | 26.7 | 90.0 |
| **4** | 6.69 | 7.21 | 7.50 | 7.13 | 520.8 | 8.1 | 33.0 | 130.0 |
| **5** | 6.53 | 5.93 | 6.40 | 6.29 | 475.2 | 6.9 | 32.2 | 120.0 |
| **6** | 5.91 | 6.05 | 6.85 | 6.27 | 447.9 | 6.6 | 22.9 | 70.0 |
| **7** | 7.86 | 6.38 | 8.61 | 7.62 | 515.4 | 8.7 | 36.1 | 140.0 |
| **8** | 6.24 | 6.08 | 6.69 | 6.34 | 558.8 | 8.9 | 15.3 | 60.0 |
| **9** | 5.58 | 5.26 | 5.42 | 5.42 | 672.2 | 8.6 | 21.7 | 110.0 |
| **10** | 5.57 | 4.94 | 5.10 | 5.20 | 670.3 | 9.8 | 18.3 | 90.0 |
| **11** | 6.58 | 7.35 | 6.42 | 6.78 | 397.1 | 5.3 | 15.6 | 40.0 |
| **12** | 5.42 | 6.53 | 6.42 | 6.12 | 504.4 | 7.8 | 16.2 | 60.0 |
| **13** | 5.42 | 5.73 | 6.05 | 5.73 | 574.3 | 9.1 | 22.1 | 100.0 |
| **14** | 6.21 | 6.53 | 5.42 | 6.05 | 524.3 | 9.1 | 16.2 | 60.0 |

**Supplementary Table 5. Diameter measurements and mechanical properties for 128-mer fibers**

| FIBER | Diam. A (μm) | Diam. B (μm) | Diam. C (μm) | Avg. Diameter (μm) | σ (MPa) | E (GPa) | ε (%) | $U_T$ (MJ/m³) |
|---|---|---|---|---|---|---|---|---|
| **1** | 7.33 | 7.05 | 6.63 | 7.00 | 874.4 | 11.4 | 39.2 | 260.0 |
| **2** | 6.56 | 7.68 | 6.03 | 6.76 | 886.1 | 9.5 | 18.9 | 100.0 |
| **3** | 7.96 | 5.47 | 5.65 | 6.36 | 650.2 | 8.4 | 12.7 | 50.0 |
| **4** | 7.49 | 5.87 | 6.00 | 6.45 | 652.1 | 8.0 | 29.5 | 150.0 |
| **5** | 4.98 | 3.54 | 4.66 | 4.39 | 642.9 | 12.9 | 9.5 | 40.0 |
| **6** | 7.18 | 6.42 | 7.07 | 6.89 | 877.2 | 12.6 | 33.3 | 200.0 |
| **7** | 6.76 | 6.91 | 6.34 | 6.67 | 654.3 | 9.0 | 19.4 | 80.0 |
| **8** | 5.77 | 5.74 | 6.55 | 6.02 | 843.0 | 9.5 | 16.8 | 90.0 |
| **9** | 6.36 | 6.53 | 5.75 | 6.21 | 816.2 | 10.7 | 15.2 | 110.0 |
| **10** | 7.01 | 6.85 | 7.66 | 7.17 | 750.4 | 9.6 | 22.0 | 90.0 |
| **11** | 7.91 | 7.91 | 7.37 | 7.73 | 744.8 | 8.2 | 27.3 | 130.0 |
| **12** | 6.41 | 5.65 | 5.59 | 5.88 | 817.5 | 11.8 | 17.4 | 90.0 |
| **13** | 6.69 | 7.50 | 8.13 | 7.44 | 717.0 | 10.7 | 25.5 | 120.0 |
| **14** | 7.41 | 8.51 | 8.20 | 8.04 | 816.7 | 12.3 | 20.0 | 100.0 |

**Supplementary Table 6. Diameter measurements and mechanical properties for 128-mer fibers**

| FIBER | Diam. A (μm) | Diam. B (μm) | Diam. C (μm) | Avg. Diameter (μm) | σ (MPa) | E (GPa) | ε (%) | $U_T$ (MJ/m³) |
|---|---|---|---|---|---|---|---|---|
| **1** | 3.02 | 3.04 | 2.75 | 2.94 | 1078.6 | 14.7 | 11.7 | 70.0 |
| **2** | 6.56 | 7.68 | 7.34 | 7.19 | 892.9 | 9.0 | 15.3 | 70.0 |
| **3** | 4.98 | 7.41 | 7.37 | 6.59 | 1034.8 | 17.8 | 28.0 | 200.0 |
| **4** | 6.91 | 6.89 | 6.72 | 6.84 | 1135.6 | 11.8 | 17.7 | 110.0 |
| **5** | 7.32 | 7.33 | 7.64 | 7.43 | 911.5 | 12.2 | 14.0 | 80.0 |
| **6** | 6.34 | 5.50 | 6.13 | 5.99 | 1324.6 | 18.9 | 27.2 | 220.0 |
| **7** | 3.19 | 3.38 | 3.06 | 3.21 | 1130.5 | 17.2 | 15.6 | 100.0 |
| **8** | 5.25 | 5.89 | 5.10 | 5.41 | 982.8 | 10.5 | 18.4 | 100.0 |
| **9** | 4.80 | 5.12 | 5.81 | 5.24 | 987.6 | 10.3 | 24.6 | 140.0 |
| **10** | 5.73 | 5.73 | 7.01 | 6.16 | 1003.0 | 14.3 | 12.2 | 70.0 |
| **11** | 5.65 | 5.91 | 6.15 | 5.90 | 961.7 | 14.5 | 21.8 | 140.0 |
| **12** | 5.78 | 5.91 | 5.92 | 5.87 | 1016.0 | 11.9 | 12.1 | 70.0 |
| **13** | 6.53 | 5.89 | 5.57 | 6.00 | 1016.6 | 13.1 | 12.8 | 70.0 |
| **14** | 5.09 | 5.29 | 4.94 | 5.11 | 952.4 | 15.2 | 24.3 | 160.0 |

**Supplementary Table 7. Quantification of morphological differences between fibers of different molecular weight.**

| Fiber | Circularity | Surface Roughness | Interior Roughness |
|---|---|---|---|
| **96-mer** | 0.55 ± 0.14 | 4.17 ± 0.68 | 8.17 ± 0.98 |
| **128-mer** | 0.82 ± 0.10 | 1.75 ± 0.69 | 7.17 ± 0.75 |
| **192-mer** | 0.89 ± 0.05 | 1.08 ± 0.58 | 5.08 ± 0.80 |

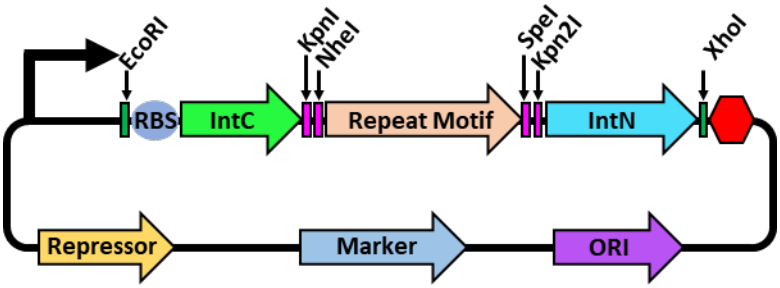


**Supplementary Figure 1. SI-Bricks assembly system.** The SI-Bricks assembly system allows for iterative assembly of repeat motifs through back-to-back NheI/SpeI digestion/ligation (Supplementary Figure 2). Assembled PBM parts are swapped with KpnI/Kpn2I digestion/ligation, $Int^C$ parts (including start codon and RBS) are swapped with EcoRI/KpnI digestion/ligation, and $Int^N$ parts are swapped with Kpn2I/XhoI digestion/ligation.

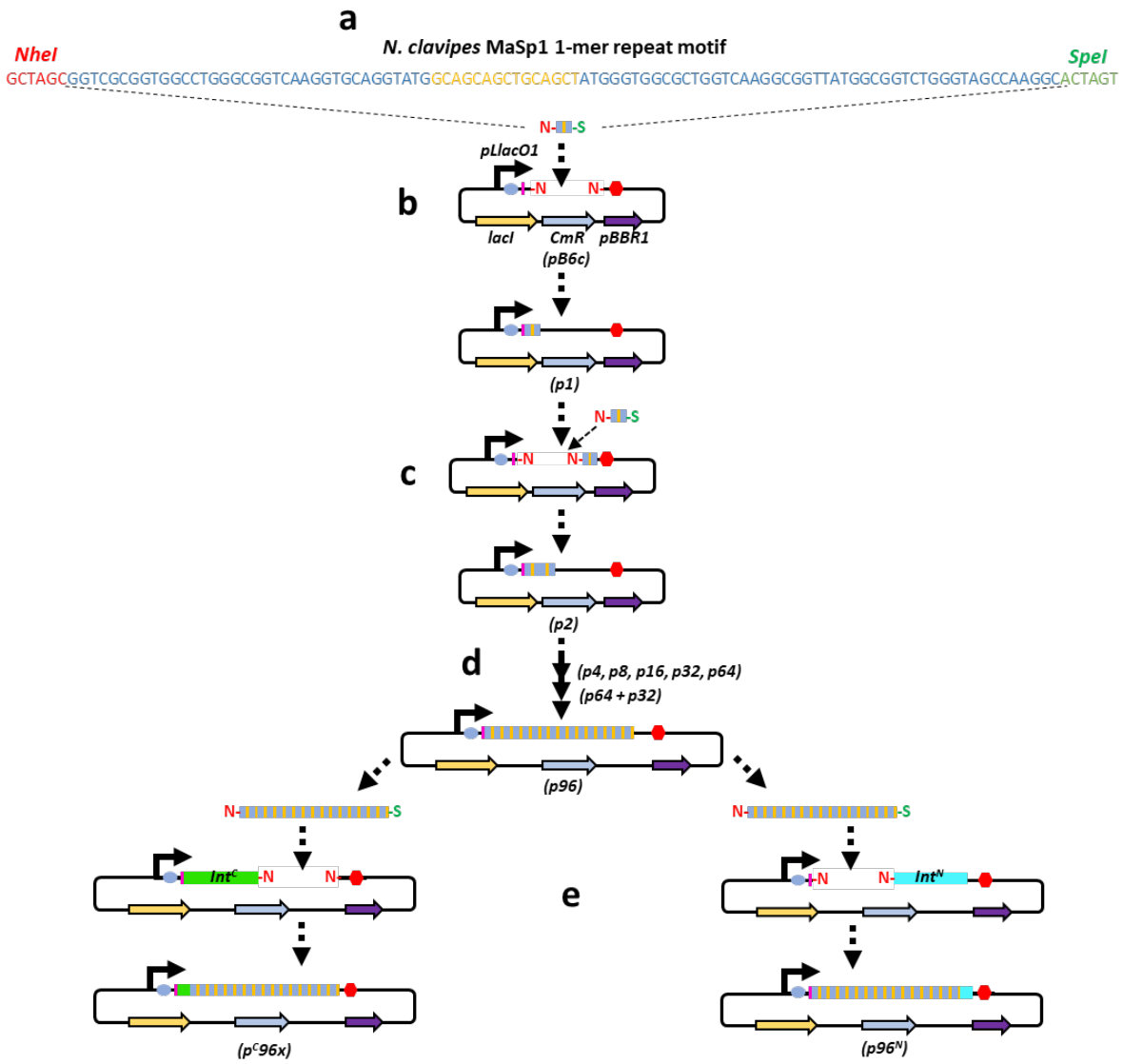


**Supplementary Figure 2. Schematic of iterative assembly of plasmids. (a)** The optimized coding sequence for a single representative repeat unit (1-mer) of the *N. clavipes* dragline silk MaSp1 protein is flanked by restriction sites NheI (N) and SpeI (S). **(b)** The sequence is ligated into the BglBricks vector pB6c with IPTG-inducible promoter pLlacO1, replication origin pBBR1, and chloramphenicol resistance $Cm^R$. **(c)** After selection for correct insert orientation, the resulting 1-mer plasmid (p1) is linearized by digestion with SpeI. The linearized vector is ligated with 1-mer insert to yield p2. **(d)** The process is repeated, each time with a two-fold larger insert until p64 is obtained. Plasmid p96 was obtained by inserting NheI/SpeI digested 32-mer into linearized p64. **(e)** The 96-mer is then inserted either 5' of optimized $Int^N$ to yield $p96^N$ or 3' of optimized $Int^C$ to yield $p^C96$.

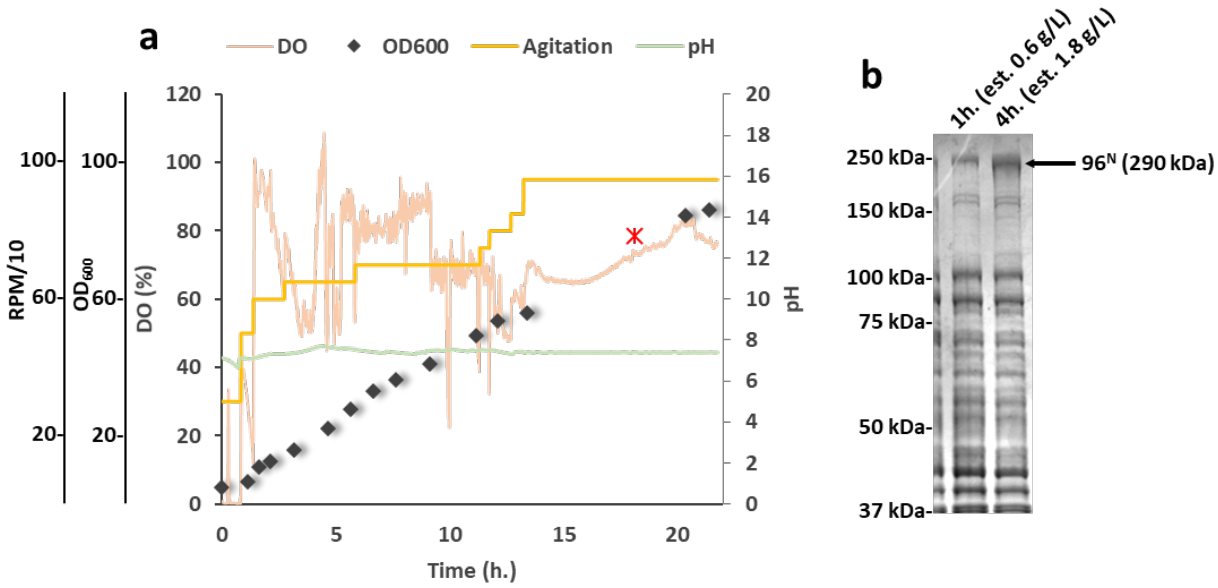


**Supplementary Figure 3. Bioproduction of spidroins in fed-batch bioreactor. (a)** Dissolved oxygen (DO), cell density ($OD_{600}$), bioreactor agitation rate, and pH over the course of fermentation. Time 0 represents the start of fermentation in the bioreactor. The red asterisk indicates the point of induction with 1 mM IPTG. **(b)** Representative SDS-PAGE of spidroin-producing cells ($96^N$) at 1 and 4 h post induction. Estimated titers of $96^N$ are indicated above each lane. Titers were estimated based on densitometric analysis of the SDS-PAGE gel as described in the methods.

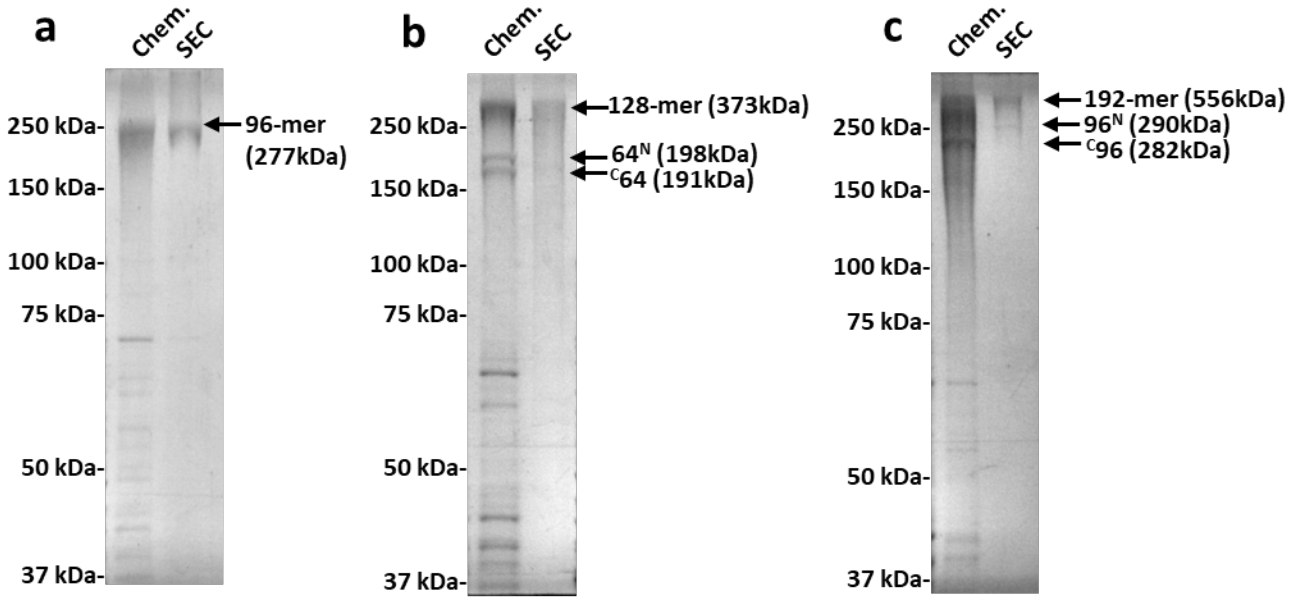


**Supplementary Figure 4. Purification of 96, 128, and 192-mer spidroins.** Coomassie Blue stained SDS-PAGE gels for purification of **(a)** 96-mer, **(b)** 128-mer, **(c)** 192-mer. Lane 1, products after selective precipitation with ammonium sulfate. Lane 2, products after SEC purification.

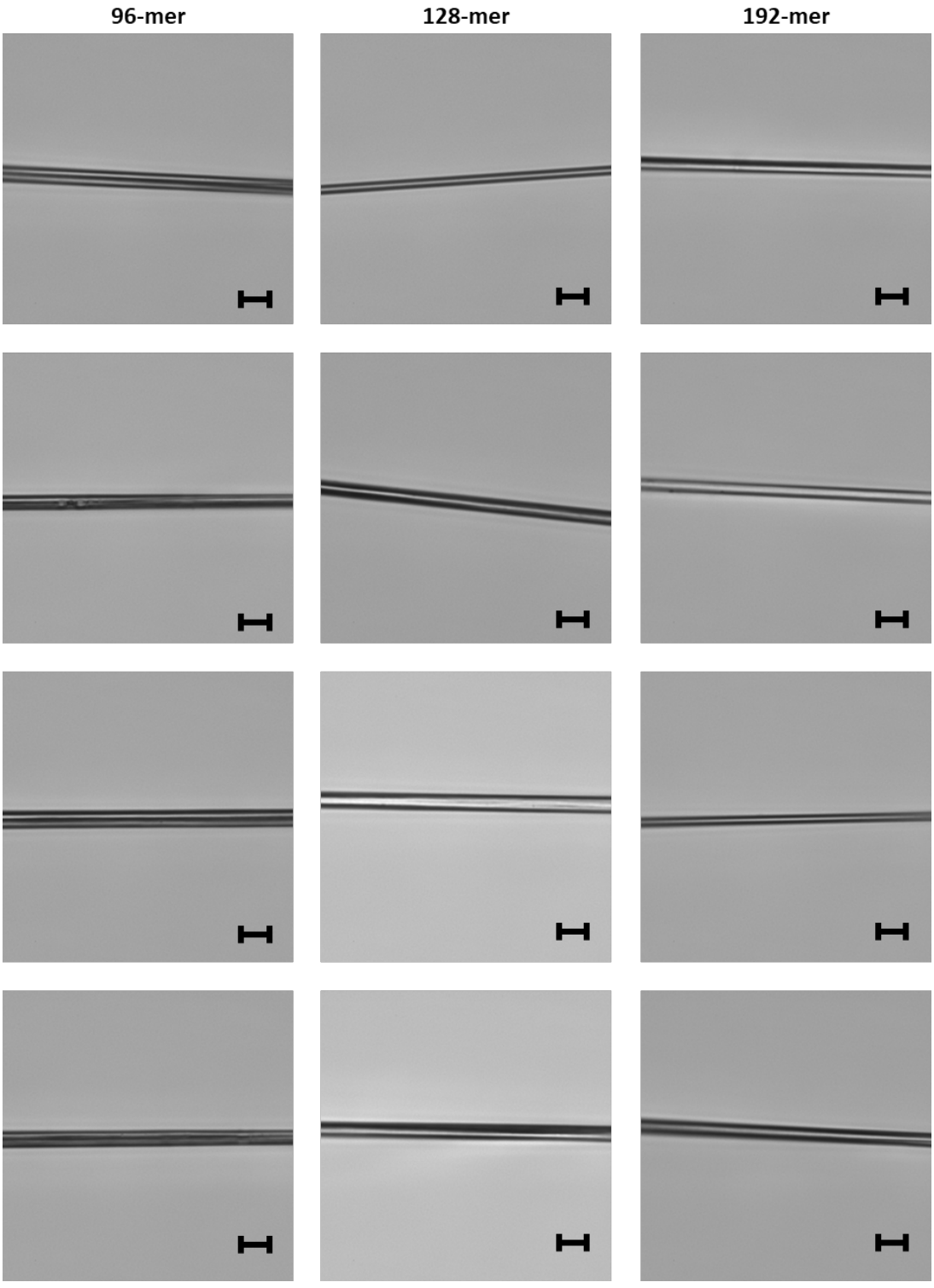


**Supplementary Figure 5. Light microscopy of spun spidroin fibers.** Representative images of spidroin fibers were recorded using a Nikon Eclipse TiE Inverted Microscope and a 60x objective. Scale bar is 5 µm.

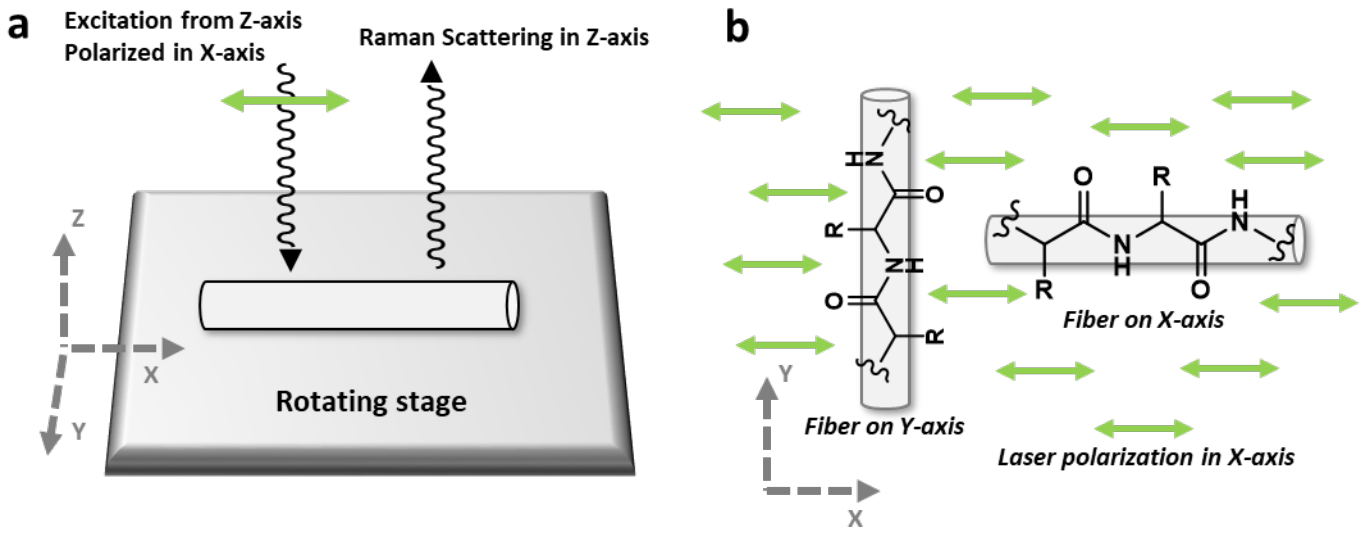


**Supplementary Figure 6. Polarized Raman microspectroscopy. (a)** Schematic representation of the apparatus from a side view. The fiber is mounted along the X-axis of a rotating stage. A laser polarized in the X-axis is directed to the fiber along the Z-axis. Raman scattering is collected along the Z-axis. **(b)** Schematic representation of polarized light interaction with fibers oriented along the Y-axis (left) or X-axis (right)**.** If peptide chains are aligned with the fiber axis (as depicted), carbonyl bonds will be maximally aligned with laser polarization when fibers are oriented along the Y-axis and minimally aligned when fibers are oriented along the X-axis. Because absorbance in the amide I band is due primarily to carbonyl stretching, an increase in 1670 $cm^{-1}$ peak intensity when fibers are oriented along the Y-axis is indicative of β-sheet alignment parallel to the fiber axis. Thus, the normalized peak intensity ratio ($I\frac{Y}{X}$) is indicative of the degree of orientation.

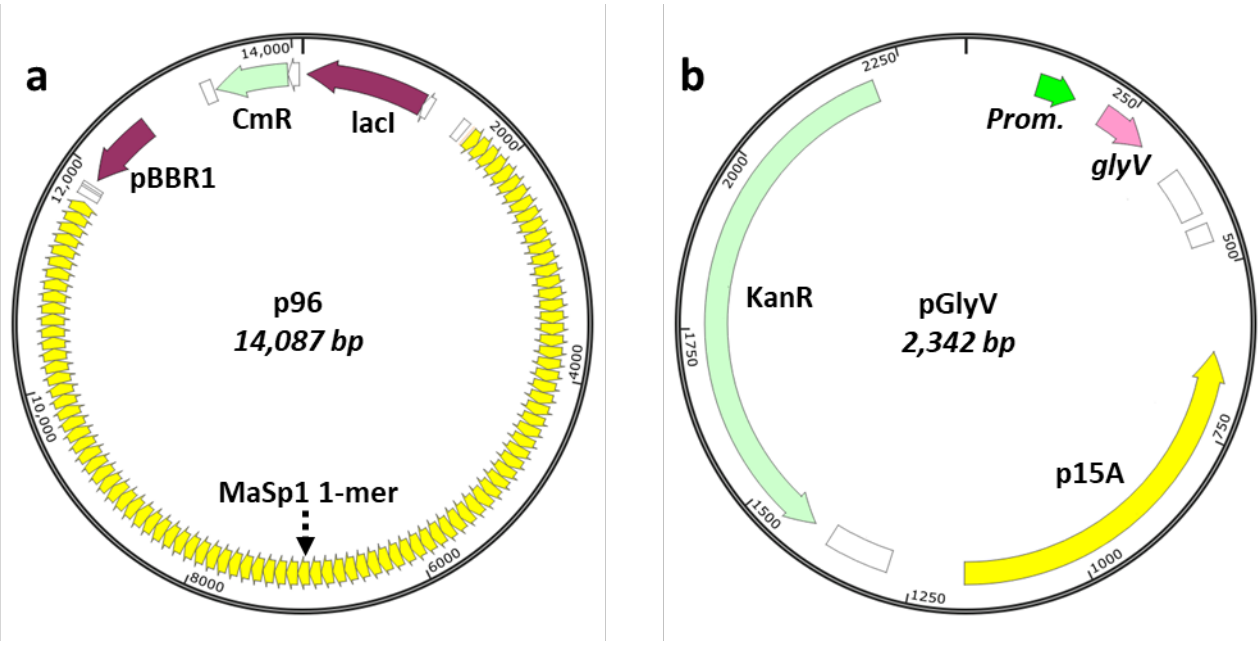


**Supplementary Figure 7. p96 and pGlyV plasmid maps.** "Prom." indicates native *E. coli* glyV,X,Y promoter.

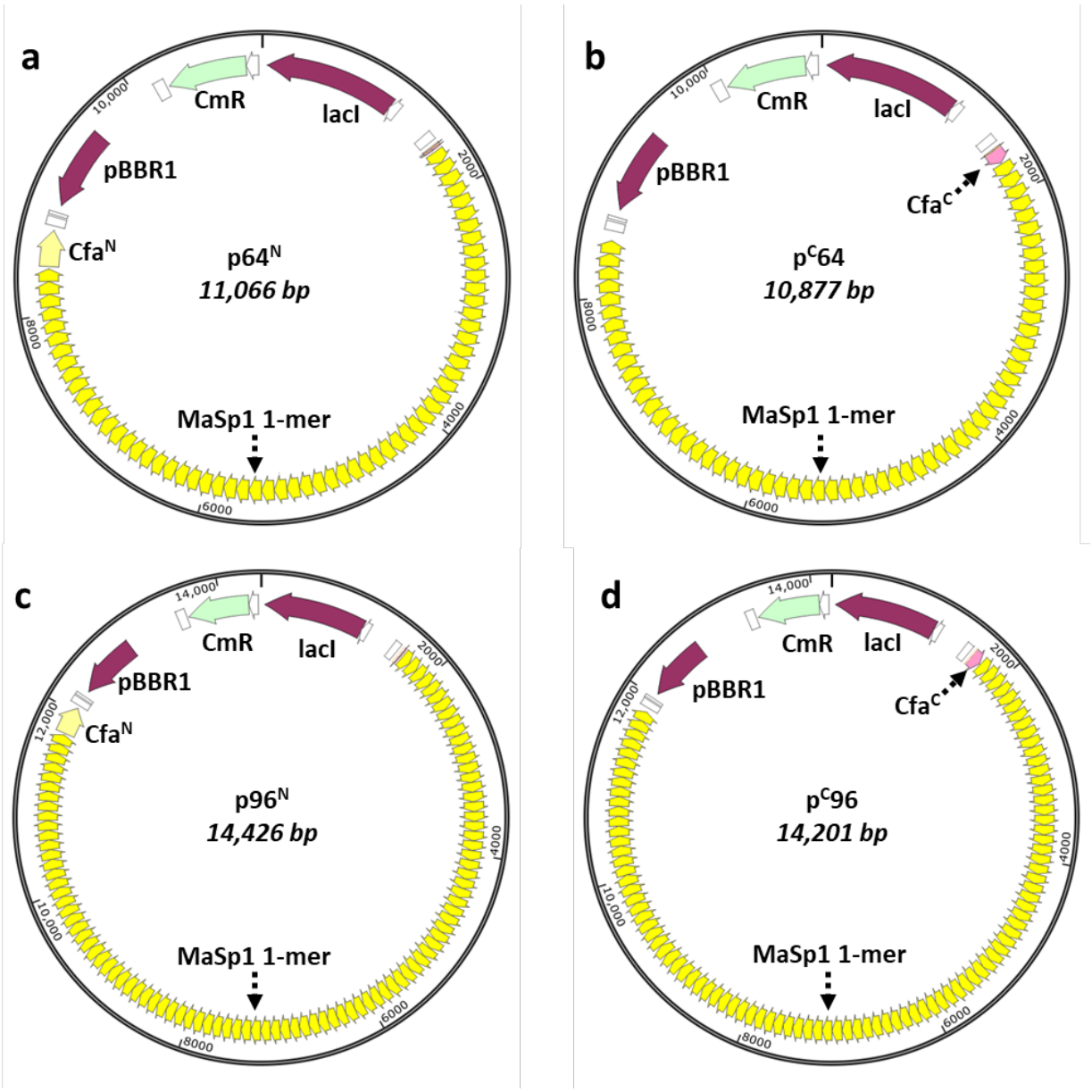


**Supplementary Figure 8. Plasmid maps for $p64^N$ (a), $p^C64$ (b), $p96^N$ (c), $p^C96$ (d).**

**REFERENCES:**

1. Anderson, J. C. *et al.* BglBricks: A flexible standard for biological part assembly. *J. Biol. Eng.* **4,** 1–12 (2010).